

Comparative Studies of $V_{1-x}Cr_xN$ Films Deposited by Conventional Magnetron Sputtering and Plasma Enhanced Magnetron Sputtering

Yanan ZHAI ^a, Zhiqiang FU ^{b,1}, Wen YUE ^b, Jiajie KANG ^b, Lina ZHU ^b and Shuo LU ^a

^aChina United Test and Certification Co., LTD, Beijing 101400, China

^bChina University of Geosciences Beijing, Beijing 100083, China

Abstract. $V_{1-x}Cr_xN$ films were deposited via conventional magnetron sputtering (CMS) and plasma enhanced magnetron sputtering (PEMS) by controlling the power of Cr target and V target. The microstructure of films was characterized using scanning electron microscope, meanwhile, the thickness was measured. The chemical composition was analyzed by an energy dispersive spectrometer, and phase structure was analyzed by X-ray diffractometer. The hardness and Young's modulus of films were evaluated using nano-indenter. With an increase in Cr content, the deposition rate increased gradually and then reduced in both $V_{1-x}Cr_xN$ films. As Cr content increased, CMS- $V_{1-x}Cr_xN$ films transformed from a mixture of FCC-V(Cr)N and FCC-VN with non-stoichiometric ratio to a mixture of FCC-V(Cr)N and BCC-Cr, and Cr content had no effect on the phase structure of PEMS- $V_{1-x}Cr_xN$ films, all of them shown FCC-V(Cr)N. In addition, the dominant texture in $V_{1-x}Cr_xN$ films deposited by CMS and PEMS were (111) and (200). As increasing Cr content, the density of the CMS- $V_{1-x}Cr_xN$ films increased gradually, moreover, all films were loose and porous. However, the Cr content had little effect on microstructure of PEMS- $V_{1-x}Cr_xN$ films, all of which shown dense columnar structure. With the increase of Cr content, the hardness and Young's modulus of CMS- $V_{1-x}Cr_xN$ films increased gradually and then decreased, while which in PEMS- $V_{1-x}Cr_xN$ films were rise. The doping of Cr significantly improves the structure and mechanical properties of CMS- $V_{1-x}Cr_xN$ films. Furthermore, the structure of PEMS- $V_{1-x}Cr_xN$ films is much denser, and the mechanical properties of PEMS- $V_{1-x}Cr_xN$ films are significantly better than CMS- $V_{1-x}Cr_xN$ films.

Keywords. Conventional magnetron sputtering, plasma enhanced magnetron sputtering, $V_{1-x}Cr_xN$ film, Cr content, structure and property

1. Introduction

The transition metal nitride films have been widely applied to surface strengthening, such as cutters and molds, due to their high melting point, high hardness, excellent thermal stability and corrosion resistance [1-3]. In recent years, VN film has attracted increasing interests attributed to its self-lubricating, it is easily oxidized to form solid vanadium oxides with a very low friction coefficient at high temperatures [4-6].

¹ Zhiqiang FU, Corresponding author, China University of Geosciences Beijing, Beijing 100083, China; E-mail: fuzq@cugb.edu.cn.

However, with the increasingly severe application environment, the mechanical properties of VN film need to be further improved. At present, a variety of measures to improve the performance of VN film have been studied, for example, optimized process parameters [7], doped alloy elements (C, Si) [8, 9], adopted nano-multilayer film structure (VN/C, TiAlN/VN) [10, 11]. Studies have shown that doping Cr into VN film could effectively improve its performance [12].

Physical vapor deposition is commonly used in thin film preparation, including magnetron sputtering, arc ion plating, ion beam assisted deposition, and other technologies. Among them, magnetron sputtering has attracted attention due to its low deposition temperature, fewer film defects, and superior film-substrate adhesion strength [13]. During film deposition via magnetron sputtering, the density and distribution of plasma would significantly affect energy and flux of ion impingement on the substrate surface, which would usefully modify structure and properties of the film [14, 15]. Generally, in conventional magnetron sputtering (CMS), the magnetron plasma with low density was controlled in a limited space in front of the target, the particles arrived substrate surface with lower energy to migrate and diffuse, which resulted in a loose and porous film. Different from CMS, an electron source and a discharge power supply were used in plasma enhanced magnetron sputtering (PEMS) to generate global plasma with higher density, independent of the magnetron plasma, in the entire vacuum system. Attributed to the enhanced ion bombardment on growing film, the growth of grains was limited, meanwhile, additional energy is transferred to particles so that adatoms could move or diffuse into the inter-grain voids [16, 17]. Therefore, the films prepared by PEMS show dense structure and excellent properties. In this study, $V_{1-x}Cr_xN$ films were deposited through CMS and PEMS by sputtering V and Cr metal targets with varied target power in a closed filed unbalanced magnetron sputtering system. The effect of Cr content on composition, structure, mechanical properties of both $V_{1-x}Cr_xN$ films were contrastively discussed.

2. Experimental

$V_{1-x}Cr_xN$ films were deposited on Si (100) wafers, which were ultrasonically cleaned in acetone before placed in sputtering chamber. When the vacuum system was pumped below a base pressure of 2.0×10^{-4} Pa, argon was passed into chamber. And then adjust the heating current at ~ 20 A and discharge voltage at -80 V, the tungsten wires were heated to emit a great number of hot electrons to generate a high-density Ar^+ plasma. Ar^+ plasma was utilized to etch substrates surface for 90 min in order to remove residual contamination before deposition. $V_{1-x}Cr_xN$ films were deposited by CMS and PEMS for 120 min by varying V and Cr target power (0~4 kV). During deposition, a substrate bias voltage of -100 V was used, Ar and N_2 flow rate were kept at 60 sccm, and substrates temperature was maintained at 300 °C. The target power of $V_{1-x}Cr_xN$ films deposition were showed in table 1.

The phase structure of $V_{1-x}Cr_xN$ films was analyzed via X-ray diffraction (XRD, Smartlab, Rigaku) with Cu-K α radiation source, and the measurements with 4 °/min were done in the range of 2θ angles from 10 ° to 90 °. The surface and cross-sectional micro-morphologies of $V_{1-x}Cr_xN$ films were characterized through a field-emission scanning electron microscope (FESEM, JSM-7610FPlus, Jeol), at the same time, the thickness of films was measured. The chemical composition was obtained using an energy dispersive spectroscope (EDS, Genesis, EDAX) attached to FESEM. The

hardness and Young's modulus were evaluated using a nano-indenter (XP, Agilent). The hardness and Young's modulus were calculated according to the load-displacement curves, in addition, the indentation depth was 120 nm.

Table 1. V and Cr target power of $V_{1-x}Cr_xN$ films.

Sample ID	$V_{1-x}Cr_xN-1$	$V_{1-x}Cr_xN-2$	$V_{1-x}Cr_xN-3$	$V_{1-x}Cr_xN-4$	$V_{1-x}Cr_xN-5$	$V_{1-x}Cr_xN-6$
V target power/kW	4	4	3	2	1	0
Cr target power/kW	0	1	2	3	4	4

3. Results and Discussion

3.1. Deposition Rate

The deposition rates of $V_{1-x}Cr_xN$ films deposited by CMS and PEMS are showed in table 2. It clearly shows that the deposition rates of both $V_{1-x}Cr_xN$ films show a trend of gradually increasing first and then decreasing slightly. This phenomenon is related to the sputtering yield of V and Cr target: the sputtering yield of Cr target is higher than V target [18], this means more Cr atoms were sputtered from target at same target power, therefore, the deposition rate of CrN film was higher than VN film [19]. As Cr target power increased from 0 to 4 kW and V target power decreased from 4 kW to 0 kW, the total number of sputtered atoms increased, and the deposition rate of $V_{1-x}Cr_xN$ film increased gradually. When V and Cr target power were 0 and 4 kW, the total target power was reduced and sputtered atoms was decreased, and the deposition rate of $V_{1-x}Cr_xN$ films was slightly reduced. In addition, it also could be seen that the deposition rate of PEMS- $V_{1-x}Cr_xN$ films was lower than CMS- $V_{1-x}Cr_xN$ films at same process conditions, which was related to the difference in film density.

Table 2. Deposition rate (nm/min) of $V_{1-x}Cr_xN$ films deposited by CMS and PEMS.

Sample ID	$V_{1-x}Cr_xN-1$	$V_{1-x}Cr_xN-2$	$V_{1-x}Cr_xN-3$	$V_{1-x}Cr_xN-4$	$V_{1-x}Cr_xN-5$	$V_{1-x}Cr_xN-6$
CMS	7.917	9.500	8.667	9.250	10.500	9.417
PEMS	3.250	4.083	5.500	6.833	7.833	7.417

3.2. Chemical Composition

Table 3 shows the chemical composition of $V_{1-x}Cr_xN$ films prepared by CMS and PEMS. At same target power, Cr content ($x=Cr/V+Cr$) and N content (at.%) in PEMS- $V_{1-x}Cr_xN$ films were close to CMS- $V_{1-x}Cr_xN$ films. With the increase of Cr target power and the decrease of V target power, the number of Cr sputtered atoms gradually increased, and the number of V sputtered atoms gradually decreased, resulting in Cr content increasing and V content reducing in both of $V_{1-x}Cr_xN$ films. Furthermore, as Cr target power increased and V target power decreased, the number of sputtered atoms gradually increased, and more N atoms participate in the reaction at same nitrogen flow. Therefore, the N relative content in both of $V_{1-x}Cr_xN$ films show a decline trend.

Table 3. Chemical composition of $V_{1-x}Cr_xN$ films deposited by CMS and PEMS.

Sample ID	CMS		PEMS	
	x=Cr/V+Cr	N/at.%	x=Cr/V+Cr	N/at.%
$V_{1-x}Cr_xN$ -1	0	60.81	0	61.53
$V_{1-x}Cr_xN$ -2	0.434	53.22	0.367	57.78
$V_{1-x}Cr_xN$ -3	0.627	54.13	0.609	56.13
$V_{1-x}Cr_xN$ -4	0.797	52.71	0.780	56.02
$V_{1-x}Cr_xN$ -5	0.918	54.29	0.913	55.77
$V_{1-x}Cr_xN$ -6	1	52.08	1	52.31

3.3. Crystal Structure

The XRD patterns of $V_{1-x}Cr_xN$ films prepared by CMS and PEMS are shown in figure 1. All films exhibit a FCC-V(Cr)N phase with a NaCl-type structure, attributed to the similar atomic radius and electronegativity of V and Cr, thus Cr atoms doping in VN would form a substitutional solid solutions [20]. For CMS- $V_{1-x}Cr_xN$ films, when the Cr content was 0~0.434, the films consist of FCC-V(Cr)N and FCC-VN_{0.81}. In Cr content range of 0.627 to 1, the $V_{1-x}Cr_xN$ films was composed of FCC-V(Cr)N and BCC-Cr. However, the Cr content had no effect on phase structure of $V_{1-x}Cr_xN$ films prepared by PEMS, and all of them were FCC-V(Cr)N.

It's worth noting that the dominant texture in $V_{1-x}Cr_xN$ films deposited by CMS and PEMS was (111) and (200). The reason is that (111) and (200) plane is the lowest strain and surface energy plane respectively in FCC-V(Cr)N films, according to energy mechanism, polycrystalline films growth is expected to show orientations which minimize total energy consisting of the surface energy and the strain energy [21]. Due to the lower energy of particles in CMS, the growth process was primarily governed by kinetics, moreover, (111) plane seems to be a favorable accommodation of large amounts of N atoms at high nitrogen flow (60 sccm), thus $V_{1-x}Cr_xN$ films mainly grew along the (111) plane preferentially [22]. It is clear that (200) reflection showed higher intensity than (111) reflection in PEMS- $V_{1-x}Cr_xN$ films, as depicted in figure 1. This is because that the nuclear stopping cross section is the largest and the smallest for (111) and (200) oriented grains in V(Cr)N, respectively [23]. On the basis of sputtering theory, the sputter yield changes along with nuclear stopping cross section, therefore, the preferential sputtering of atoms in (111) planes were intensified by high ion bombardment, which restricted the orientation of grains. In contrast, grains with a (200) orientation had the smallest nuclear stopping cross section and the lowest sputtering yield would grow [24, 25].

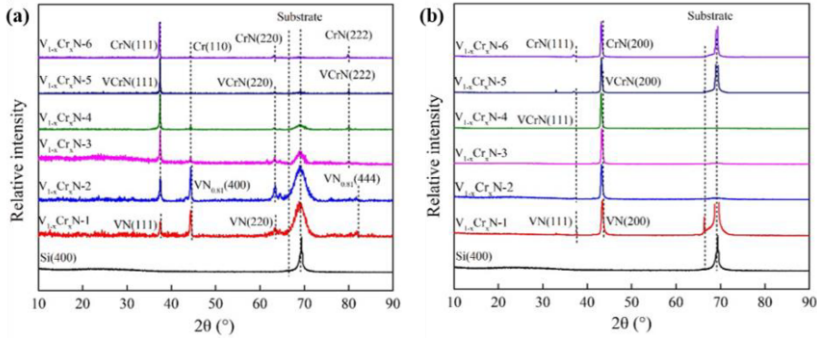


Figure 1. XRD patterns of $V_{1-x}Cr_xN$ films deposited by CMS (a) and PEMS (b).

3.4. Microstructure

The surface SEM micrographs are showed in figure 2. For CMS- $V_{1-x}Cr_xN$ films, when Cr content was low (0~0.434), the films showed a quadrangular pyramid surface morphology with loose structure and high porosity. With the further increase of Cr content (0.627~1), the porosity of films was decreased gradually, showing a morphology with triangular pyramids. Such triangular pyramids surface morphology was corresponding to the films showed a FCC-V(Cr)N (111) preferred orientation [26]. For PEMS- $V_{1-x}Cr_xN$ films, however, there was few effect of Cr content on microstructure, all of them showed a smooth surface with no pores.

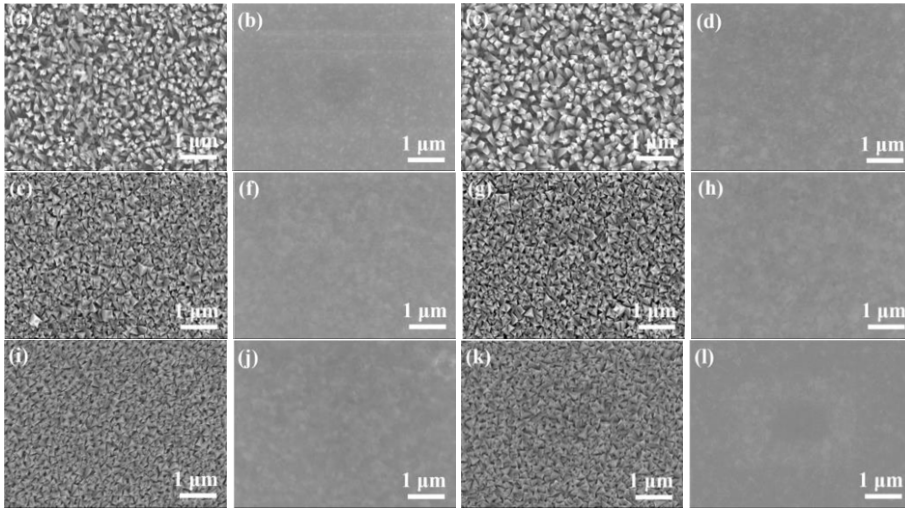


Figure 2. Surface SEM micrographs of $V_{1-x}Cr_xN$ films deposited by CMS (a, c, e, g, i, k) and PEMS (b, d, f, h, j, l): $V_{1-x}Cr_xN-1$ (a, b), $V_{1-x}Cr_xN-2$ (c, d), $V_{1-x}Cr_xN-3$ (e, f), $V_{1-x}Cr_xN-4$ (g, h), $V_{1-x}Cr_xN-5$ (i, j), $V_{1-x}Cr_xN-6$ (k, l).

The cross-sectional SEM micrographs are showed in figure 3. The microstructure of CMS- $V_{1-x}Cr_xN$ films showed a transition structure between the Ic and T Zone in Mahieu model, and each columnar grain grew independently and through entire thickness [27]. As shown in figure 3 (a) and (c), it can be seen that the doping of Cr has

significantly improved the structure of CMS-V(Cr)N films, and the film density has been obviously increased. With the increase of Cr content (0.627~1), the films showed a denser structure, and the pores between the columnar gradually decreased. In addition, from the cross-sectional morphologies of CMS- $V_{1-x}Cr_xN$ films, it can be observed that the structure at film initial growth was relatively dense and the grains were fine, and the structure at film later growth was loose and the grains were coarse. In initial stage of film growth (0~200 nm), the films were dense because of more nucleation sites, however, due to the limited migration and diffusion of particles in CMS, each columnar grew independently in the later stage of film growth. The Cr content had almost no effect on the cross-sectional morphology of PEMS- $V_{1-x}Cr_xN$ films, all of them were dense and exhibited typical Zone T columnar structure [27].

According to the comparative analysis of microstructure of both $V_{1-x}Cr_xN$ films, it is found that the films prepared by PEMS had a denser structure, finer grains and fewer defects. This difference in microstructure can be explained by ion bombardment. During the deposition process, ion bombardment could promote the densification of film [15]. In PEMS, the ion/atom arrival ratio was high, it means that the flux ratio of ions and atoms reaching the substrate was higher [28], as bombardment ion transferred energy to the adparticles on substrate, the adparticles had enough energy to migrate or diffuse to grain boundaries and vacancies. In CMS, the ion/atom arrival was lower, and the mobility of the adparticles was low, each crystal could only grow epitaxially to form columnar, therefore, the film was loose and there were defects such as pores between columnar. The difference in microstructure of both $V_{1-x}Cr_xN$ films was the main reason that the deposition rate of CMS- $V_{1-x}Cr_xN$ films was significantly higher than PEMS- $V_{1-x}Cr_xN$ films.

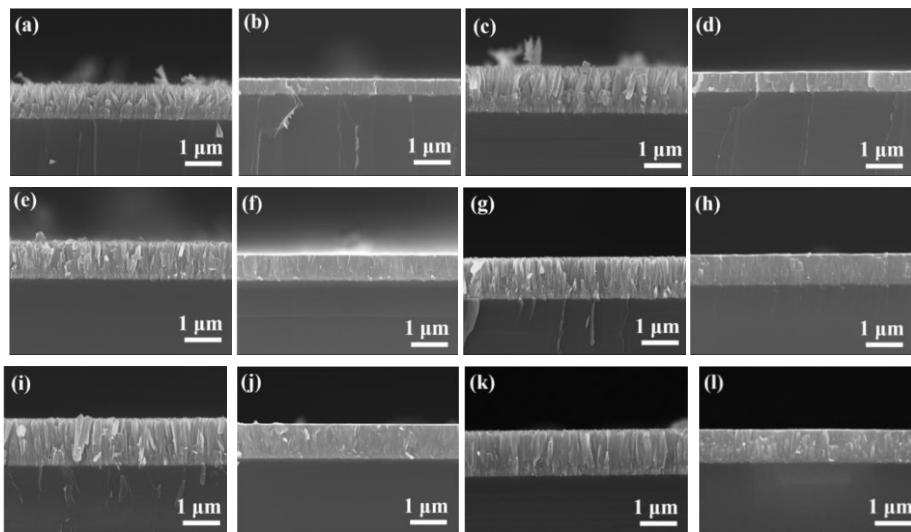


Figure 3. Cross-sectional SEM micrographs of $V_{1-x}Cr_xN$ films deposited by CMS (a, c, e, g, i, k) and PEMS (b, d, f, h, j, l): $V_{1-x}Cr_xN$ -1 (a, b), $V_{1-x}Cr_xN$ -2 (c, d), $V_{1-x}Cr_xN$ -3 (e, f), $V_{1-x}Cr_xN$ -4 (g, h), $V_{1-x}Cr_xN$ -5 (i, j), $V_{1-x}Cr_xN$ -6 (k, l).

3.5. Mechanical Property

The mechanical properties of $V_{1-x}Cr_xN$ films prepared by CMS and PEMS are shown in figure 4. The doping of Cr significantly improved the mechanical properties of CMS- $V_{1-x}Cr_xN$ films. With the increase of Cr content, the hardness and Young's modulus were elevated gradually and then decreased slightly. The main reason that the mechanical properties of the CMS- $V_{1-x}Cr_xN$ films were improved was attributed to the denser microstructure. In addition, the solid solution hardening effect caused by difference in atomic radius contributed to the increase in mechanical properties of CMS- $V_{1-x}Cr_xN$ films. As Cr content increased, hardness and Young's modulus of PEMS- $V_{1-x}Cr_xN$ films also showed a rise. The higher density and finer grain resulted in the enhancement of mechanical properties, however, higher residual stress generated from higher ion bombardment was also an important factor [29].

The hardness and Young's modulus of PEMS- $V_{1-x}Cr_xN$ films were significantly higher than CMS- $V_{1-x}Cr_xN$ films, which was mainly related to microstructure. PEMS- $V_{1-x}Cr_xN$ films had dense structure and fine grain, while CMS- $V_{1-x}Cr_xN$ films exhibited typical columnar crystal with pores and other defects.

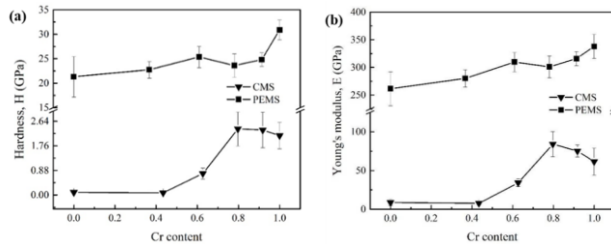


Figure 4. Mechanical properties of the $V_{1-x}Cr_xN$ films deposited by PEMS and CMS: Hardness (a), Young's modulus (b).

4. Conclusion

The influence of Cr content on structure and property of $V_{1-x}Cr_xN$ films deposited by conventional magnetron sputtering and plasma enhanced magnetron sputtering was explored. With the increase of Cr target power and the decrease of V target power, the Cr content of both $V_{1-x}Cr_xN$ films increased gradually, and the deposition rate firstly increased and then decreased slightly. The deposition rate of CMS- $V_{1-x}Cr_xN$ films is greater than PEMS- $V_{1-x}Cr_xN$ films. CMS- $V_{1-x}Cr_xN$ films changed from a mixed phase of FCC-VN_{0.81} and FCC-V(Cr)N to a mixed phase of FCC-V(Cr)N and BCC-Cr. In PEMS- $V_{1-x}Cr_xN$ films, there is no effect of Cr content on phase structure, and all films show FCC-V(Cr)N. The dominant texture in $V_{1-x}Cr_xN$ films deposited by PEMS and CMS are V(Cr)N (111) and V(Cr)N (200), respectively. The density of CMS- $V_{1-x}Cr_xN$ films gradually increases as Cr content was increase, and films were loose and porous columnar structure, which exhibit the transition structure between Ic and T Zone in Mahieu model. The Cr content had few effects on the microstructure of PEMS- $V_{1-x}Cr_xN$ films, all of them were dense and exhibited typical Zone T zone columnar structure. Cr significantly enhanced the mechanical properties of both $V_{1-x}Cr_xN$ films. The hardness and Young's modulus of CMS- $V_{1-x}Cr_xN$ films gradually increase firstly and then slightly decrease with the increase of Cr content. The mechanical properties of

PEMS- $V_{1-x}Cr_xN$ films show a rise as the Cr content was increased. The mechanical properties of PEMS- $V_{1-x}Cr_xN$ films are significantly better than that of CMS- $V_{1-x}Cr_xN$ films.

Reference

- [1] Kong, DJ, Fu, GZ, Zhang, L, et al. Friction and wear properties of AlCrN coating by cathodic arc ion plating. *Rare Metals*. 2021; 40(5): 1300-1306.
- [2] He, CL, Zhang, JL, Xie, LP, et al. Microstructure, mechanical and corrosion properties of TiN/Ni nanomultilayered films. *Rare Metals*. 2019; 38(10): 979-988.
- [3] Cui, WF, Dong, YY, Bao, YC, et al. Improved corrosion resistance of dental Ti50Zr alloy with (TiZr)N coating in fluoridated acidic artificial saliva. *Rare Metals*. 2021; 40(10): 2927-2936.
- [4] Wu CK, Huang JH, Yu GP. Optimization of deposition processing of VN thin films using design of experiment and single-variable (nitrogen flow rate) methods. *Materials Chemistry and Physics*. 2019; 224: 246-256.
- [5] Fateh N, Fontalvo GA, Gassner G, et al. Influence of high-temperature oxide formation on the tribological behaviour of TiN and VN coatings. *Wear*. 2007; 262(9-10): 1152-1158.
- [6] Hajihoseinia H, Kateb M, Ingvarsson S, et al. Effect of substrate bias on properties of HiPIMS deposited vanadium nitride films. *Thin Solid Films*. 2018; 663: 126-130.
- [7] Caicedo JC, Zambrano G, Aperador W, et al. Mechanical and electrochemical characterization of vanadium nitride (VN) thin films. *Applied Surface Science*. 2011; 258(1): 312-320.
- [8] Caicedo JC, Aperador W, Amaya C. Determination of physical characteristic in vanadium carbon nitride coatings on machining tools. *The International Journal of Advanced Manufacturing Technology*. 2017; 91: 1227-1241.
- [9] Huang F, Ge F, Zhu P, et al. Superhard V-Si-N coatings (> 50 GPa) with the cell-like nanostructure prepared by magnetron sputtering. *Surface and Coating Technology*. 2013; 232: 600-605.
- [10] Liu ZX, Li Y, Xie XH, et al. The tribo-corrosion behavior of monolayer VN and multilayer VN/C hard coatings under simulated seawater. *Ceramics International*. 2021; 47(18): 25655-25663.
- [11] Mayrhofer PH, Hovsepian PE, Mitterer C, et al. Calorimetric evidence for frictional self-adaptation of TiAlN/VN superlattice coatings. *Surface and Coating Technology*. 2004; 177-178: 341-347.
- [12] Rapoport L, Moshkovich A, Perfilyev V, et al. High temperature friction behavior of CrVxN coatings. *Surface and Coating Technology*. 2014; 238: 207-215.
- [13] Yu DH, Wang CY, Cheng XL, et al. Recent development of magnetron sputtering processes. *Vacuum*; 2009, 46: 19-25.
- [14] Matossian J, Wei R, Vajo J, et al. Plasma-enhanced, magnetron-sputtered deposition (PMD) of materials. *Surface and Coating Technology*. 1998; 108-109: 496-506.
- [15] Petrov I, Barna PB, Hultman L, et al. Microstructural evolution during film growth. *Journal of Vacuum Science & Technology A Vacuum Surfaces & Films*. 2003; 21(5): S117-S128.
- [16] Wei R, Langa E, Rincon C, et al. Deposition of thick nitrides and carbonitrides for sand erosion protection. *Surface and Coating Technology*. 2006; 201: 4453-4459.
- [17] Wei R, Vajo JJ, Matossian JN, et al. Aspects of plasma-enhanced magnetron-sputtered deposition of hard coatings on cutting tools. *Surface and Coating Technology*. 2002; 158: 465-472.
- [18] Tian MB, Li ZC. *Film technologies and film materials*. Beijing: Tsinghua University Press, 2011.
- [19] Qiu Y, Zhang S, Li B, et al. Improvement of tribological performance of CrN coating via multilayering with VN. *Surface and Coating Technology*. 2013; 231: 357-363.
- [20] Yu X, Hu C, Li C, et al. Effect of V-addition on the thermal stability and oxidation resistance of CrAlN coatings. *Ceramics International*. 2018; 44(6): 7013-7019.
- [21] Lee JW, Tien SK, Kuo YC. The effects of substrate bias, substrate temperature, and pulse frequency on the microstructures of chromium nitride coatings deposited by pulsed direct current reactive magnetron sputtering. *Journal of Electronic Materials*. 2005; 34(12): 1484-1492.
- [22] Kong Q, Li J, Li H, et al. Composition, microstructure, and properties of CrNx films deposited using medium frequency magnetron sputtering. *Applied Surface Science*. 2011; 257(6): 2269-2274.
- [23] Daniel R, Martinschitz KJ, Keckes J, et al. Texture development in polycrystalline CrN coatings: the role of growth conditions and a Cr interlayer. *Journal of Physics D Applied Physics*. 2009; 42(7): 075401.
- [24] He XM, Baker N, Kehler BA, et al. Structure, hardness, and tribological properties of reactive magnetron sputtered chromium nitride films. *Journal of Vacuum Science & Technology A Vacuum Surfaces & Films*. 2000; 18(1): 30-36.

- [25] Zhao ZB, Rek ZU, Yalisove SM, et al. Phase formation and structure of magnetron sputtered chromium nitride films: in-situ and ex-situ studies. *Surface and Coatings Technology*, 2004; 185(2-3): 329-339.
- [26] Inoue S, Okada F, Koterazawa K. CrN films deposited by RF reactive sputtering using a plasma emission monitoring control. *Vacuum*, 2002; 66(3-4): 227-231.
- [27] Mahieu S, Ghekiere P, Depla D, et al. Biaxial alignment in sputter deposited thin films. *Thin Solid Films*. 2006; 515(4): 1229-1249.
- [28] Kelly PJ, Arnell RD. Magnetron sputtering: a review of recent developments and applications. *Vacuum*. 2000; 56(3): 159-172.
- [29] Zou CW, Wang HJ, Li M, et al. Characterization and properties of CrN films deposited by ion-source-enhanced middle frequency magnetron sputtering. *Vacuum*. 2009; 83(8): 1086-1090.